Generating Overcritical Dense Relativistic Electron Beams via Self-Matching Resonance Acceleration

B. Liu,[1] H. Y. Wang,[1] J. Liu,[2] L. B. Fu,[2] Y. J. Xu,[1] X. Q. Yan,[1,*] and X. T. He[1,2,†]

[1]*Key Laboratory of HEDP of the Ministry of Education, CAPT, and State Key Laboratory of Nuclear Physics and Technology, Peking University, Beijing 100871, China*
[2]*Institute of Applied Physics and Computational Mathematics, Beijing 100088, China*

We show a novel self-matching resonance acceleration regime for generating dense relativistic electron beams by using ultraintense circularly polarized laser pulses in near-critical density plasmas. When the self-generated quasistatic axial magnetic field is strong enough to pinch and trap thermal relativistic electrons, an overdense electron bunch is formed in the center of the laser channel. In the trapping process, the electron betatron frequencies and phases can be adjusted automatically to match the resonance condition. The matched electrons are accelerated continuously and a collimated electron beam with overcritical density, helical structure, and plateau profile energy spectrum is hence generated.

The rapid development of ultraintense laser technology has opened new and active research fields in laser plasma interactions [1] ranging from fast ignition of inertial confinement fusion [2], laboratory astrophysics [3], to development of compact sources of high-energy particles, such as electrons, ions, and gamma photons [4,5].

In laser plasma interactions, the resonance between betatron motion of electrons and ultraintense laser pulses is an interesting phenomenon and attracts much attention in both electron acceleration [6,7] and gamma photon production [5]. A betatron oscillating relativistic electron, confined by the self-generated quasistatic transverse fields, can be resonant with the laser pulse and gain energy efficiently from the laser fields. This is an inverse process of the ion-channel laser [8]. In order to accelerate electron beam in such a way, the resonance condition must be realized: the frequency and phase of the electron betatron motion should be matched with the laser pulse in the electron comoving frame. However, by using linearly polarized (LP) laser pulses, the preacceleration process necessary to reach the resonant behavior is stochastic in nature, and only few electrons experience the betatron resonance acceleration [9], which severely limits the density and number of energetic electrons, and lacks practical applications.

In this Letter, by using ultraintense circularly polarized (CP) laser pulses in near-critical density plasmas, we report on a novel self-matching resonance acceleration (SMRA) regime, where the electron betatron frequencies and phases are adjusted automatically to match the resonance condition. In such ultraintense and near-critical conditions, the self-generated quasistatic magnetic fields play an important role in many phenomena, including the relativistic magnetic self-channeling of light [10], magnetic-dipole vortex generation [11], ion acceleration by magnetic field annihilation [12], and laser shaping by plasma lens [13]. In

particular, quasistatic axial magnetic fields can be generated by CP laser pulses, which have been widely investigated both theoretically and experimentally [14]. In the presence of axial magnetic field, electron acceleration by CP laser pulses shows interesting and complex properties [15,16]. With the aid of analytical modeling and 3D simulations, we found that when the self-generated quasistatic axial magnetic field is strong enough to pinch and trap the thermal relativistic electrons, an overdense electron bunch can appear in the center of the plasma channel produced by the laser pulse. In this process, the frequencies and phases of the trapped electrons can be self-matched with that of the laser pulse in the electron comoving frame, and the resonance conditions are satisfied. The matched electrons exhibit similar behavior: executing betatron rotation around the axial magnetic field and being accelerated continuously along the laser propagation direction. Hence a collimated relativistic electron beam with overcritical density and helical structure is generated.

In the CP laser evacuated channel, strong quasistatic magnetic fields, both in the axial and azimuthal direction are generated. The self-generated axial magnetic field B_{Sz} provides a "trapping effect" on relativistic electrons. An upper bound of perpendicular momentum for the trapped electrons is defined, when the radius of the Larmor motion is equal to the spot size of the axial magnetic field, as

$$p_{\text{tr}} = 2eRB_{Sz}, \tag{1}$$

where p_{tr} is called trapping momentum, R is the radius of the spot size of the axial magnetic field, and e is the elementary charge. On the other hand, the quasistatic azimuthal magnetic field produces a "resonance effect." In order to understand the mechanism of the resonance, we employ the single-particle dynamics model, which has been widely investigated in many similar problems [17]. It is noticed that, in near critical density plasmas, the

collective behavior of the electrons may begin to modify the dynamics away from what one obtains from single-particle orbits alone [18]. In the LP laser field, the collective behavior may cause density asymmetry in the perpendicular direction, while in our CP laser case, since the laser field is symmetrical, such collective effects are negligible. Considering a right-hand CP plane wave with frequency ω_0, the transverse electromagnetic fields are $E_{Lx} = E_L \cos\phi$, $E_{Ly} = E_L \sin\phi$, $B_{Lx} = -E_{Ly}/v_{ph}$, $B_{Ly} = E_{Lx}/v_{ph}$, where $\phi = kz - \omega_0 t$, $v_{ph} = \omega_0/k$ is the phase velocity, and k is the wave number. The self-generated quasistatic azimuthal magnetic field can be expressed as $\boldsymbol{B}_{S\theta} = -B_{Sy}\boldsymbol{i} + B_{Sx}\boldsymbol{j}$. For an electron moving in combination with the self-generated quasistatic magnetic field (both in axial and azimuthal direction) and the laser pulse, the equations of the transverse motion are $dp_x/dt = -e\kappa E_L \cos\phi + ev_z B_{Sy} - ev_y B_{Sz}$, $dp_y/dt = -e\kappa E_L \sin\phi - ev_z B_{Sx} + ev_x B_{Sz}$, where $\kappa = 1 - v_z/v_{ph}$. It is difficult to solve the equations analytically without any approximation. We focus on the resonance electrons, for which the longitudinal velocity v_z and the Lorentz factor γ are slow variables compared to the fast variables p_x and p_y. It is resonable to assume that $\dot{v}_z \rightarrow 0$ and $\dot{\gamma} \rightarrow 0$. According to the circular symmetry of the azimuthal magnetic field, we have $\partial B_{S\theta}/\partial r = -\partial B_{Sy}/\partial x = \partial B_{Sx}/\partial y$. Then the derivative of the equations becomes

$$\frac{d^2 p_x}{dt^2} + \Omega_\theta^2 p_x + \Omega_z \frac{dp_y}{dt} = m_e c a_L \omega_L^2 \sin\omega_L t, \quad (2)$$

$$\frac{d^2 p_y}{dt^2} + \Omega_\theta^2 p_y - \Omega_z \frac{dp_x}{dt} = m_e c a_L \omega_L^2 \cos\omega_L t, \quad (3)$$

where $a_L = eE_L/m_e c\omega_0$ is the normalized laser amplitude, $\omega_L = \kappa\omega_0$ is the frequency of the laser pulse in the electron comoving frame, $\Omega_\theta = \sqrt{\frac{ev_z}{\gamma m_e}\frac{\partial}{\partial r}B_{S\theta}}$, $\Omega_z = eB_{Sz}/\gamma m_e$, and m_e, c are the electron mass and the speed of light in vacuum, respectively. By ignoring small oscillating terms, the transverse momenta can be solved as $p_x(t) = -p_\perp(t)\cos\omega_+ t$, $p_y(t) = p_\perp(t)\sin\omega_+ t$, where the perpendicular momentum is

$$p_\perp(t) = \frac{2m_e c a_L \omega_L^2}{(\omega_B - \omega_L)(\omega_B + \omega_L + \Omega_z)} \sin\omega_- t \quad (4)$$

and the frequency of the betatron motion $\omega_B = \sqrt{\Omega_\theta^2 + (\Omega_z/2)^2} - \Omega_z/2$, here $\omega_+ = (\omega_B + \omega_L)/2$, $\omega_- = (\omega_B - \omega_L)/2$. It is clearly seen that resonance occurs when $\omega_B \approx \omega_L$.

The resonance acceleration of electrons in CP laser pulses is usually investigated under the condition of $\gamma \gg 1$ (e.g., in Ref. [16]). However, the axial magnetic field B_{Sz} contributes only a small quantitative modification to the resonance effect, and is negligible when $\gamma \gg 1$.

In this sense, we can say that the resonance effect is dominated by the azimuthal magnetic field $B_{S\theta}$. On the other hand, in the trapping effect, the axial magnetic field B_{Sz} plays a crucial role. In order to understand the electron dynamics comprehensively, we must investigate the transition process from the trapping regime to the resonance regime. If an electron is initially trapped in the self-generated quasistatic axial magnetic field B_{Sz}, the only way to escape is to make the amplitude of the perpendicular momentum described in Eq. (4) exceed the trapping momentum p_{tr}, i.e.,

$$\left| \frac{2m_e c a_L \omega_L^2}{(\omega_B - \omega_L)(\omega_B + \omega_L + \Omega_z)} \right| > 2eRB_{Sz}, \quad (5)$$

or

$$\frac{\Delta\omega}{\omega_L} < \left(1 + \frac{\Omega_z}{2\omega_L}\right)\left(\sqrt{1 + \frac{m_e c a_L}{eRB_{Sz}}\bigg/\left(1 + \frac{\Omega_z}{2\omega_L}\right)^2} - 1\right), \quad (6)$$

where $\Delta\omega = |\omega_B - \omega_L|$. When the axial magnetic field is strong enough to make

$$\frac{m_e c a_L}{eRB_{Sz}}\bigg/\left(1 + \frac{\Omega_z}{2\omega_L}\right)^2 \ll 1, \quad (7)$$

we have

$$\frac{\Delta\omega}{\omega_L} < \frac{a_L}{2\pi(R/\lambda)[(B_{Sz}/B_0)^2 + 2(B_{Sz}/B_0)]}, \quad (8)$$

where $B_0 = m_e\omega_0/e$, $\lambda = 2\pi c/\omega_0$, and $\gamma\kappa \sim 1$ is taken for the trapped electrons. The stronger the axial magnetic field B_{Sz}, the closer the right-hand side of Eq. (8) is to zero, i.e., $\Delta\omega/\omega_L \rightarrow 0$, which means that only exactly matched electrons can escape. Since the trapped electrons are driven by the rapidly varying laser fields, they have enough opportunity to adjust their frequencies and phases to match the resonance conditions. The trapping effect of the axial magnetic field and the resonance effect of the azimuthal magnetic field together develop a self-matching mechanism. In this situation, the trapped electrons form a "reservoir", which provides resonance electrons continually.

To investigate the features of SMRA, we carried out simulations using a fully relativistic three-dimensional (3D) particle-in-cell (PIC) code (KLAP) [19]. A right-hand CP laser beam with central wavelength $\lambda = 1\ \mu$m, wave period $T = \lambda/c$, rise time $5T$, peak intensity $I_0 = 5 \times 10^{20}$ W/cm^2, and spot diameter 4 μm (FWHM), is normally incident from the left boundary ($z = 0$) of a $80 \times 16 \times 16\ \mu$m^3 simulation box with a grid of $960 \times 192 \times 192$ cells. A near-critical density plasma target consisting of electrons and protons is located in 6 μm $< z <$ 77 μm. In the laser propagation direction, the plasma density rises linearly from 0 to $n_0 = n_c$ in a distance of 5 μm, and then remains constant, where $n_c = m_e\omega_0^2\epsilon_0/e^2$ is the critical plasma density, and ϵ_0 is the vacuum permittivity. In the

radial direction, the density is uniform. The number of particles used in the simulation is 5×10^8 for each species (16 particles per cell for each species corresponds to n_0). An initial electron temperature T_e of 150 keV is used to resolve the initial Debye length ($T_i = 10$ eV initially).

Simulation results at $t = 80T$ are plotted in Fig. 1. The incident laser beam first propagates through an unstable filamentary stage and then collapses into a single channel, which is known as relativistic magnetic self-channeling [10], as is shown in Fig. 1(a) in the longitudinal cut. Both electrons and ions are expelled by the self-focused laser pulse. The unique feature here is that a high density electron beam is generated in the center of the laser channel, as is shown in Fig. 1(b), where the beam is labeled by a black dashed box. The radius of the beam is less than 1 μm, while the radius of the channel is about 3 μm. The maximum density of the beam is up to $3n_c$, which is
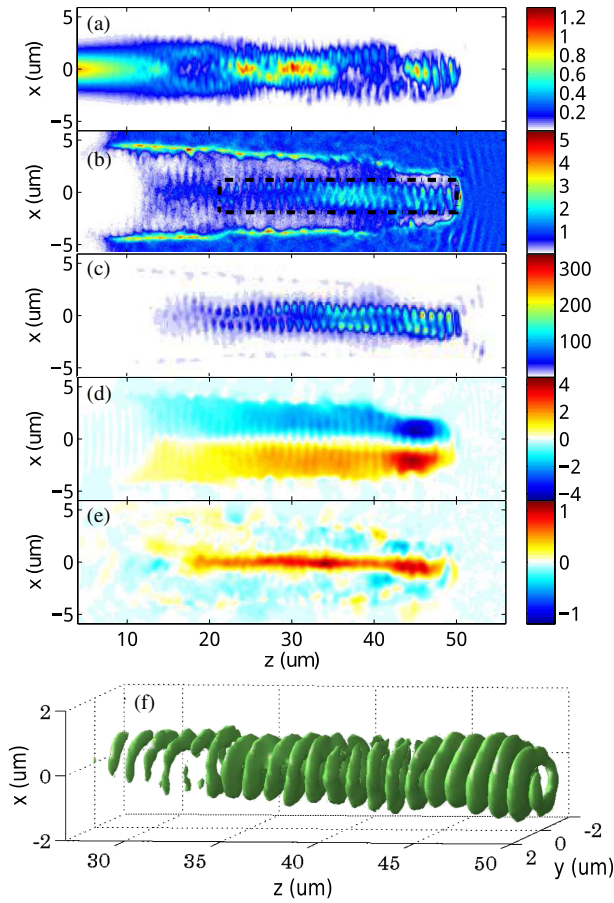
FIG. 1 (color online). Simulation results at $t = 80T$. (a)–(e) Longitudinal (Z, X) cuts along the pulse axis of, (a) instantaneous laser intensity I, normalized by the initial intensity $I_0 = 5 \times 10^{20}$ W/cm^2; (b) electron density n_e, normalized by the critical density n_c; (c) electron energy density normalized by $n_c m_e c^2$; (d), (e) self-generated azimuthal and axial magnetic fields $B_{S\theta}$ and B_{Sz}, averaged over laser period, normalized by $m_e \omega_0/e$. (f) 3D isosurface distribution of electron energy density with isosurface value $100 n_c m_e c^2$.

far greater than the initial density of the plasma. Most of the energy of the electrons is localized in the beam, as is shown by the energy density distribution in Fig. 1(c). The points with the maximum energy density are distributed at the edge of the beam. The self-generated quasistatic azimuthal and axial magnetic fields are shown in Figs. 1(d) and 1(e). In the simulation, the self-focused laser intensity is close to its initial value; then we can use $a_L \sim 13.4$. The axial magnetic field $B_{Sz} \sim 1.4 B_0$, with the radius of the spot size $R \sim 0.8$ μm, is strong enough to make the frequency of the betatron motion satisfy $\Delta \omega / \omega_L < 0.6$. Figure 1(f) plots the isosurface of the energy density with isosurface value $100 n_c m_e c^2$ in 3D, which shows a helical structure with the same period as the laser pulse.

In order to illustrate SMRA in detail the evolutions for a resonance electron of the perpendicular momentum $p_\perp$, the radius of motion r, the Lorentz factor γ, the perpendicular velocity $v_\perp$, and the frequencies ω_B and ω_L, are plotted in Figs. 2(a)–2(e). The electron is first dragged into the center of the channel from the channel boundary by the self-generated fields. In the center of the channel, the evolution can be divided into two processes, the trapping process (I), and the resonance process (II). In the trapping process, the electron, with a lower perpendicular momentum $p_\perp < p_{tr}$, is trapped by the quasistatic axial magnetic field. There is no obvious energy gain when the electron is trapped. The frequency of the betatron motion ω_B and the frequency of the laser pulse in the electron comoving frame ω_L both vary rapidly. When the resonance condition is achieved, i.e., the frequencies and phases are matched, the evolution goes into the resonance process. In the resonance process, with the perpendicular momentum exceeding the trapping momentum, the electron is out of the axial magnetic field area, and into the azimuthal magnetic field dominant regime. The Lorentz factor increases dramatically until the electron catches up to the electrostatic sheath field in the front of the laser pulse at $90T$. The perpendicular velocity $v_\perp$ is suppressed to about $0.2c$. The matching of frequencies ω_B and ω_L, and the matching of the corresponding phases (the time integral of the frequency curve), are both maintained. After $100T$, the electron exceeds the front of the laser pulse in the propagation direction and moves freely. The corresponding transverse trajectory of the electron projected in the quasistatic axial magnetic field B_{Sz} is shown in Fig. 2(f). In the trapping process [marked by green line (bright)], the electron is trapped in the axial magnetic field. In the resonance process [marked by blue line (dark)], the electron is thrown out of the axial magnetic field, and then rotates around the axial magnetic field. All resonance electrons show similar dynamic properties, which can be explained by the SMRA model. In the resonance process, $\omega_B \approx \omega_L$, we have $p_\perp = m_e c a_L \omega_L t / 2$, $p_x = -p_\perp \cos \omega_L t$, and $p_y = p_\perp \sin \omega_L t$. Note that $\omega_L t \approx -\phi$; i.e., the betatron motion is synchronous with the laser pulse, which ensures that the electron is always in the acceleration phase.
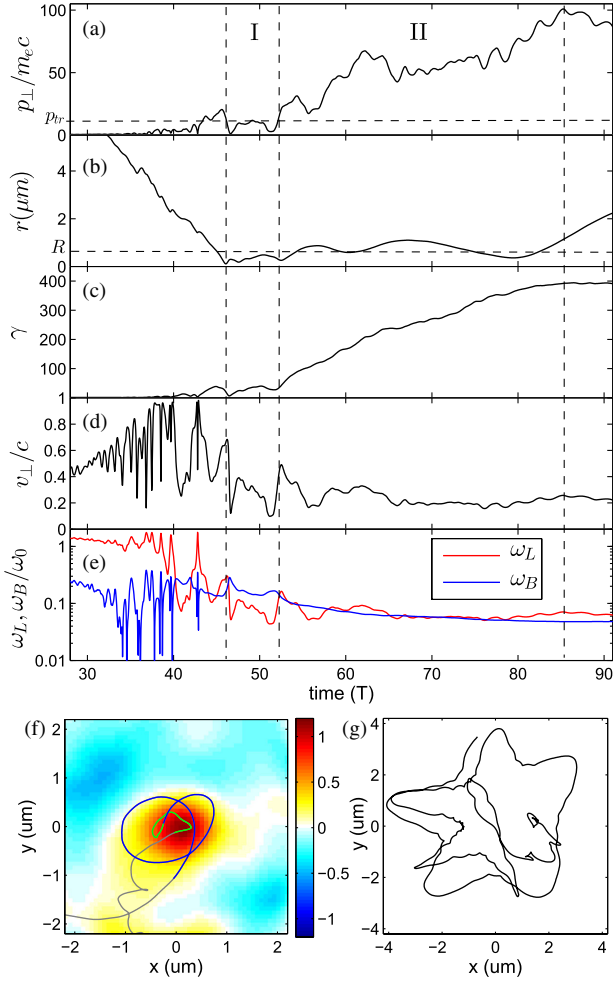
FIG. 2 (color online). Simulation results of sample electrons.
(a)–(e) The evolutions, for a resonance electron, are shown of,
(a) the perpendicular momentum $p_\perp$, normalized by $m_e c$; (b) the
radius of motion r; (c) the Lorentz factor γ; (d) the perpendicular
velocity $v_\perp$, normalized by c; (e) the frequencies ω_B and ω_L,
normalized by ω_0. The three vertical dashed lines indicate the
two processes: I, the trapping process, and II, the resonance
process. (f) The corresponding transverse trajectory of the
resonance electron projected in the quasistatic axial magnetic
field B_{Sz}. The quasistatic axial magnetic field is cut at the
position of the selected electron at $t = 50T$, normalized by
$m_e \omega_0/e$. The two processes are marked by the green line (bright)
and the blue line (dark), respectively. (g) The transverse trajec-
tory of a nonresonance electron.

By taking p_x and p_y into the energy equation $m_e c^2 d\gamma/dt =
-eE_L(p_x \cos\phi + p_y \sin\phi)/\gamma m_e$, the Lorentz factor is
determined as $\gamma = a_L \omega_0 t\sqrt{\kappa/2} + 1$. At the beginning of
the acceleration, $\gamma \approx 1$, the transverse motion is an
Archimedes' spiral. The electron is thrown out of the axial
magnetic field along a spiral trajectory. When $\gamma \gg 1$, the
perpendicular velocity $v_\perp = p_\perp/\gamma m_e \to c\sqrt{\kappa/2}$, is ap-
proximately a constant, which means that the transverse
motion is a circle. The acceleration mechanism of the

resonance electron in the self-generated azimuthal mag-
netic field is very similar to that of the original inverse
free-electron-laser accelerator by means of circularly
polarized electromagnetic waves in static helical magnet
field [20]. Since the axial magnetic field is generated by the
transverse rotating electrons, the radius of the circle is equal
to the radius of the spot size of the axial magnetic field, thus
$R = v_\perp/\omega_B \to \lambda/2\pi\sqrt{2\kappa}$, and the self-generated axial
magnetic field is estimated as $B_z = R\mu_0 e n_e v_\perp =
n_e B_0/2n_c$, where n_e is the density of the electron beam.
The transverse trajectory of a nonresonance electron is
shown in Fig. 2(g). For the nonresonance electron, when it
passes through the center of the channel, the perpendicular
momentum is too large to allow the electron to be trapped by
the axial magnetic field. The amplitude of the transverse
motion of the nonresonance electron is about 3 μm, which
is almost the radius of the channel.

Figure 3(a) shows the time evolution of the maximum
electron energy, which increases dramatically soon after
the laser irradiates on the plasma and reaches a saturation
value 240 MeV after $100T$. The energy spectrum of the
electrons at $t = 100T$ shows a rather plateau profile energy
spectrum, as is shown in Fig. 3(b). The angular distribution
of electron energy is plotted in Fig. 3(c), which shows that
the divergence angle (full angle) of the high energy elec-
trons is about 0.15 rad and the peak of the angle distribution
is at 0.2 rad, suggesting that the output electron beam is
highly collimated and the accelerated electrons are execut-
ing collective betatron motion with perpendicular velocity
$\langle v_\perp \rangle \sim 0.2c$. The SMRA model predicts a divergence
angle (full angle) of the accelerated electrons, $\Delta\theta =
(\langle v_\perp \rangle/c)(\Delta\omega/\omega_L) \sim 0.12$ rad, which agrees with the
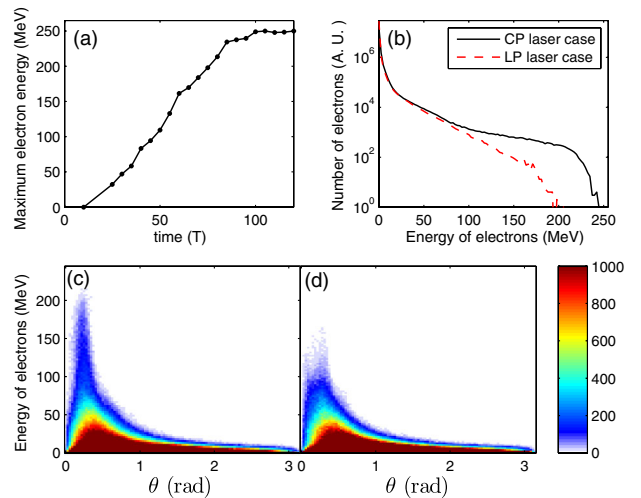
FIG. 3 (color online). (a) Time evolution of the maximum
electron energy. (b) Energy spectrum of electrons at $t = 100T$
for the CP laser pulse (black solid line) and the LP laser pulse
(red dashed line) with the same laser intensity. (c), (d) Angular
distribution of electron energy at $t = 100T$ for the CP laser pulse
and the LP laser pulse with the same laser intensity, respectively.

simulation results. In order to highlight the advantages of the SMRA regime, we compared the case by using a LP laser pulse with the same laser intensity where the quasi-static axial magnetic field is absent. The energy spectrum of electrons for the LP laser case is shown in Fig. 3(b) by a red dashed line, which shows a thermal-like distribution, as is mentioned in Ref. [6]. The angular distribution of electron energy for the LP laser case is shown in Fig. 3(d), which shows a larger divergence angle and a lower energy peak.

In summary, the SMRA regime has been proposed with the aid of analytical modeling and 3D-PIC simulations. In combination of the self-generated magnetic fields (both in axial and azimuthal direction) and the laser pulse, relativistic electrons can experience two processes: in the trapping process, the electron betatron frequencies and phases are adjusted automatically to match the resonance conditions; in the resonance process, the matched electrons are accelerated continuously along the laser propagation direction. All resonance electrons show similar dynamic behavior, which can be explained by the SMRA model. This SMRA regime, in which a collimated relativistic electron beam with overcritical density, helical structure, and plateau profile energy spectrum, can be generated, might be very promising for x-ray production or ion acceleration.

*X.Yan@pku.edu.cn

†xthe@iapcm.ac.cn

[1] G. A. Mourou, T. Tajima, and S. Bulanov, Rev. Mod. Phys. **78**, 309 (2006).

[2] M. Tabak, J. Hammer, M. E. Glinsky, W. L. Kruer, S. C. Wilks, J. Woodworth, E. M. Campbell, M. D. Perry, and R. J. Mason, Phys. Plasmas **1**, 1626 (1994); M. Roth et al., Phys. Rev. Lett. **86**, 436 (2001); V. Bychenkov, W. Rozmus, A. Maksimchuk, D. Umstadter, and C. E. Capjack, Plasma Phys. Rep. **27**, 1017 (2001); S. Atzeni, M. Temporal, and J. J. Honrubia, Nucl. Fusion **42**, L1 (2002).

[3] B. A. Remington, D. Arnett, R. Paul Drake, and H. Takabe, Science **284**, 1488 (1999); S. V. Bulanov, T. Zh. Esirkepov, D. Habs, F. Pegoraro, and T. Tajima, Eur. Phys. J. D **55**, 483 (2009).

[4] E. Esarey, C. Schroeder, and W. Leemans, Rev. Mod. Phys. **81**, 1229 (2009); T. Tajima and J. M. Dawson, Phys. Rev. Lett. **43**, 267 (1979); E. L. Clark et al., ibid. **84**, 670 (2000); A. Maksimchuk, S. Gu, K. Flippo, D. Umstadter, and V. Y. Bychenkov, ibid. **84**, 4108 (2000); A. McPherson, B. D. Thompson, A. B. Borisov, K. Boyer, and C. K. Rhodes, Nature (London) **370**, 631 (1994); S. P. Hatchett et al., Phys. Plasmas **7**, 2076 (2000).

[5] S. Cipiccia et al., Nat. Phys. **7**, 867 (2011).

[6] A. Pukhov and J. Meyer-ter-Vehn, Phys. Plasmas **5**, 1880 (1998); A. Pukhov, Z.-M. Sheng, and J. Meyer-ter-Vehn, ibid. **6**, 2847 (1999); C. Gahn, G. Tsakiris, A. Pukhov, J. Meyer-ter-Vehn, G. Pretzler, P. Thirolf, D. Habs, and K. Witte, Phys. Rev. Lett. **83**, 4772 (1999).

[7] G. D. Tsakiris, C. Gahn, and V. K. Tripathi, Phys. Plasmas **7**, 3017 (2000); D. N. Gupta and C.-M. Ryu, ibid. **12**, 053103 (2005); C. S. Liu and V. K. Tripathi, ibid. **12**, 043103 (2005); D. N. Gupta and H. Suk, ibid. **13**, 013105 (2006).

[8] D. H. Whittum, A. M. Sessler, and J. M. Dawson, Phys. Rev. Lett. **64**, 2511 (1990).

[9] See, e.g., S. P. D. Mangles et al., Phys. Rev. Lett. **94**, 245001 (2005).

[10] A. Pukhov and J. Meyer-ter-Vehn, Phys. Rev. Lett. **76**, 3975 (1996).

[11] T. Nakamura and K. Mima, Phys. Rev. Lett. **100**, 205006 (2008).

[12] Y. Fukuda et al., Phys. Rev. Lett. **103**, 165002 (2009); T. Nakamura, S. V. Bulanov, T. Z. Esirkepov, and M. Kando, ibid. **105**, 135002 (2010); S. S. Bulanov et al., Phys. Plasmas **17**, 043105 (2010).

[13] H. Y. Wang, C. Lin, Z. Sheng, B. Liu, S. Zhao, Z. Guo, Y. Lu, X. He, J. Chen, and X. Yan, Phys. Rev. Lett. **107**, 265002 (2011).

[14] Z. Najmudin et al., Phys. Rev. Lett. **87**, 215004 (2001); A. Kim, M. Tushentsov, D. Anderson, and M. Lisak, ibid. **89**, 095003 (2002); A. Frolov, Plasma Phys. Rep. **30**, 698 (2004); I. Y. Kostyukov, G. Shvets, N. J. Fisch, and J. M. Rax, Phys. Plasmas **9**, 636 (2002); S. Zhu, C. Y. Zheng, and X. T. He, ibid. **10**, 4166 (2003); B. Qiao, S.-p. Zhu, C. Y. Zheng, and X. T. He, ibid. **12**, 053104 (2005); C. Y. Zheng, X. T. He, and S. P. Zhu, ibid. **12**, 044505 (2005); N. Naseri, V. Y. Bychenkov, and W. Rozmus, ibid. **17**, 083109 (2010).

[15] H. Liu, X. T. He, and S. G. Chen, Phys. Rev. E **69**, 066409 (2004); A. Sharma and V. K. Tripathi, Phys. Plasmas **12**, 093109 (2005); B. Qiao, X. T. He, S.-p. Zhu, and C. Y. Zheng, ibid. **12**, 083102 (2005); H. Y. Niu, X. T. He, C. T. Zhou, and B. Qiao, Phys. Plasmas **16**, 013104 (2009).

[16] H. Y. Niu, X. T. He, B. Qiao, and C. T. Zhou, Laser Part. Beams **26**, 51 (2008).

[17] See, e.g., K. Németh, B. Shen, Y. Li, H. Shang, R. Crowell, K. Harkay, and J. Cary, Phys. Rev. Lett. **100**, 095002 (2008); A. V. Arefiev, B. N. Breizman, M. Schollmeier, and V. N. Khudik, ibid. **108**, 145004 (2012).

[18] L. Yin, B. Albright, K. Bowers, D. Jung, J. Fernández, and B. Hegelich, Phys. Rev. Lett. **107**, 045003 (2011); L. Yin, B. J. Albright, D. Jung, R. C. Shah, S. Palaniyappan, K. J. Bowers, A. Henig, J. C. Fernndez, and B. M. Hegelich, Phys. Plasmas **18**, 063103 (2011).

[19] X. Q. Yan, C. Lin, Z. Sheng, Z. Guo, B. Liu, Y. Lu, J. Fang, and J. Chen, Phys. Rev. Lett. **100**, 135003 (2008); Z. Sheng, K. Mima, J. Zhang, and H. Sanuki, ibid. **94**, 095003 (2005).

[20] R. B. Palmer, J. Appl. Phys. **43**, 3014 (1972).